Integrating mesh adaptivity and digital image correlation for full-field displacement evaluation of cracked bodies

Felipe L. A. Oliveira[1], Igor P. Zago[2], Vinicius F. Sciuti[3], Ricardo A. Angélico[1]

[1]*Dept. of Aeronautical Engineering, São Carlos School of Engineering, University of São Paulo*
Av. João Dagnone, 1100, Santa Angelina, 13563-120, São Carlos/SP, Brazil
felorenzo@usp.br, raa@sc.usp.br
[2]*Graduate Program in Materials Science and Engineering – PPGCEM, Federal University of São Carlos*
Rod. Washington Luis, KM 235, 13565-905, São Carlos/SP, Brazil
ipzago@estudante.ufscar.br
[3]*Dept. of Materials Engineering, Federal University of São Carlos*
Rod. Washington Luis, KM 235, 13565-905, São Carlos/SP, Brazil
vinicius.sciuti@ufscar.br

Abstract. The study of crack initiation and propagation is fundamental to the fracture mechanics and essential for establishing inspection techniques. In particular, mechanical and thermal tests are important in measuring properties and contribute to the material selection process. Such tests can be assisted by non-intrusive measurement techniques, such as Digital Image Correlation (DIC), which provides full-field information about the displacement and strain fields in a loaded configuration. Full-field information combined with numerical models enables identifying intrinsic fracture properties of the material system, which improves microstructure design and sheds light to complex deformation mechanisms. Identifying the crack position requires special treatment of the correlation process to get reasonable resolution around the crack. Finite element based DIC can benefit from mesh refinement strategies to improve the identification of the displacement field and crack location. In this paper, mesh refinement strategies were developed to improve image correlation in cracked specimens while balancing computational cost and analysis accuracy. The developed adaptive approach uses the Application Programming Interface (API) of the Gmsh software, which has several features to control the element mesh size distribution. The evaluation of the algorithm is established for reducing global gray-level residue and computational cost.

Keywords: digital image correlation, adaptive meshes, Gmsh, mechanical testing, fracture mechanics.

1 Introduction

Crack initiation and propagation monitoring are important for various structural projects, as several materials remain functional even after cracking [1]. Refractory ceramics, applied as thermal insulators in high-temperature industrial applications, are widely used materials for which the study of the cracking process is fundamental. These materials present thermal, mechanical, chemical, and electrical properties above a considerable temperature [2]. In such a context, mechanical tests carried out until fracture are essential to evaluate crack initiation and propagation [3, 4], including their evaluation in high temperatures. The identification of mechanical properties at high temperatures requires special instrumentation, which may be replaced by measurement techniques with no physical contact, such as Digital Image Correlation (DIC), which also enhances the information as a full-field technique [5]. DIC allows the identification of the displacement field and, consequently, the deformation field, from the comparison between images of the specimen in a reference condition and in a deformed configuration [6, 7]. Moreover, it enriches the information extracted from the tests, allowing verification of boundary conditions applied to the sample, monitoring experiments with complex stress states, providing information for computational models parameters identification, or even for validating them [6].

Image correlation technique can be implemented according to local or global approaches [7], being the second one used in the present paper. The global approach allows the displacement field to be approximated using a finite element mesh [8, 9]. In studying cracked specimens, it is important to have adequate refinement that provides high accuracy in the crack surroundings. Thus, there is a need for an appropriate discretization strategy for crack monitoring. Sciuti et al. [10] use non-conforming meshes to refine the discretization using two approaches: (i)

gray-level residue and (ii) Mean Crack Opening Displacement (MCOD). There is little literature on using h-refinement techniques in DIC with conformal meshes. Baldi and Bertolino [11] developed an adaptive algorithm and evaluated its performance based on the study of artificially deformed images.

The present article aims to develop mesh refinement strategies that improve DIC in cracked specimens while balancing computational cost and analysis accuracy. Herein, the developed strategies are applied using artificial images representing a cracked specimen. Meshes with uniform element size distribution are compared in terms of gray-level results and computational cost. The developments here contribute to the application of the DIC technique in cracked specimens.

2 Digital Image Correlation

Given two images, a reference image, f, and a deformed image, g, which are scalar functions that represent the gray level values of each pixel coordinate $\mathbf{x}$, and assuming that the optical flow is conserved [9]:

$$f(\mathbf{x}) = g(\mathbf{x} + \mathbf{u}(\mathbf{x})), \tag{1}$$

where $\mathbf{u}(\mathbf{x})$ represents the displacements field. If the reference image is differentiable, it is possible to use a Taylor expansion at the eq. (1), to correlate the images by minimizing the gray-level residue ϕ^2 over the region of interest Ω, i.e.

$$\phi^2 = \int_\Omega [f(\mathbf{x}) - g(\mathbf{x} - \mathbf{u}(\mathbf{x}) \cdot \nabla f(\mathbf{x}))]^2. \tag{2}$$

Herein, the displacement field is approximated using a 3-node triangular finite elements shape function (T3-shape).

All these equations were implemented in the MATLAB *software* Correli 3.2 [12], by François Hild and Stephán Roux, from "Laboratoire de Mécanique Paris-Saclay" (LMPS), and used herein.

3 Refinement strategy

The mesh generation process utilizes the Application Programming Interface (API) of the Gmsh software. By providing the average element size, it generates the corresponding triangular element mesh. However, its algorithm creates meshes with slightly variable element sizes, making it necessary to evaluate the maximum, average, and minimum values to completely characterize the mesh. Additionally, it allows for the regeneration of the mesh with a higher refinement in areas of interest in passing a background file containing the nodal coordinates of each element and a target element size, where the target value and the regions to be refined depend on the adopted refinement strategy.

The refinement strategy adopted is based on Mean Crack Opening Displacement (MCOD), $\overline{[\![u]\!]}$, as proposed by Sciuti et al. [10]. Taking the same assumptions of Sciuti et al. [10], related to the main opening distribution associated with the mode I regime and using the eigendirection linked to the average maximum eigenstrain, ε_1, MCOD can be defined as $\overline{[\![u]\!]} \doteq \ell\,\varepsilon_1$, where ℓ is the element size of the element, computed by the square root of the finite element area.

The refinement is computed as $\ell_{i+1} = \beta\,\ell_i$, where β is the refinement ratio. Only the elements with MCOD: $\overline{[\![u]\!]} > \overline{[\![u^*]\!]}$ are refined, in which $\overline{[\![u^*]\!]}$ is a threshold chosen by the user; the others maintain approximately the current size, except for some Gmsh adjustments. To refine the mesh, it is passed a background field [13] based on ℓ_{i+1}, where the Gmsh algorithm refines the elements of smaller element sizes. Additionally, it has algorithms to smooth the gradient of element sizes.

When the background field is passed to Gmsh, it is needed to translate the Correli and Gmsh element sizes, using the correspondence given by $\ell_G = 0.6385\,\ell + 0.2903$. This polynomial was obtained through linear regression between the values obtained by simulation in a range of element sizes from 1.25% to 20% of the image size.

4 Study case

The refinement strategy is demonstrated to an artificial image of a cracked body using two 1024×1024 px gray image. The deformed configuration presents a straight crack from the image center to the middle point of the

right edge, as illustrated in Fig. 1. The crack opening on the right edge is 1 px. The yellow contours represent the initial mesh, which has an average element size of 108 px. The mesh applied has dimensions 1000 x 1000 px. The elements do not present the exact same element size due to the mesh generation algorithm from Gmsh.

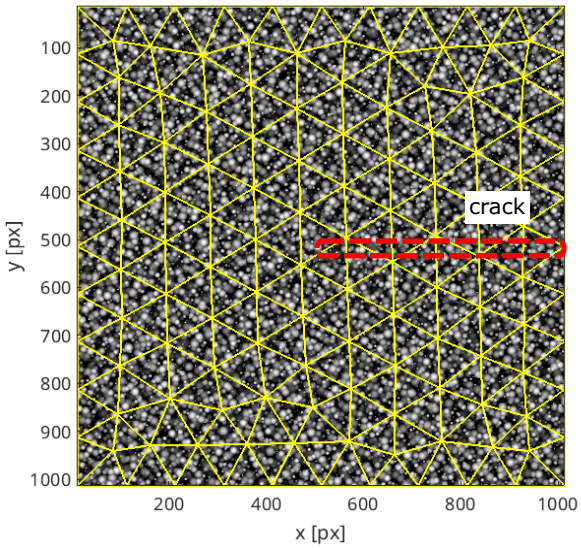

Figure 1. Initial finite element mesh (in yellow) and crack region (in red) over the deformed image ($g(\mathbf{x})$).

5 Results

The element size distribution of the initial mesh can be seen in Fig. 2 (a). The minimum and maximum element sizes are 80 px and 120 px, respectively. The MCOD has been computed, and its distribution is shown in Fig. 2 (b). The values of MCOD for each element have been used to filter which region must be refined in the next iteration. After applying the refinement strategy, a new mesh is obtained, shown in Fig. 2 (c). The minimum and maximum element sizes after the first iteration are 42 and 129 px, respectively. Adopting $\beta = 0.5$ and $[\![u^*]\!] = 0.2$, the stop criterion of $\ell_{min} = 4$ px was verified after four iterations. The initial and final mesh, obtained after four iterations, are compared in Fig. 3. The elements on the crack location were refined, as expected. The mesh presents smaller elements close to the corners in the refinement process, which is a consequence of the mesh control parameters of the Gmsh algorithm, since the background images did not predict any refinement in such regions.

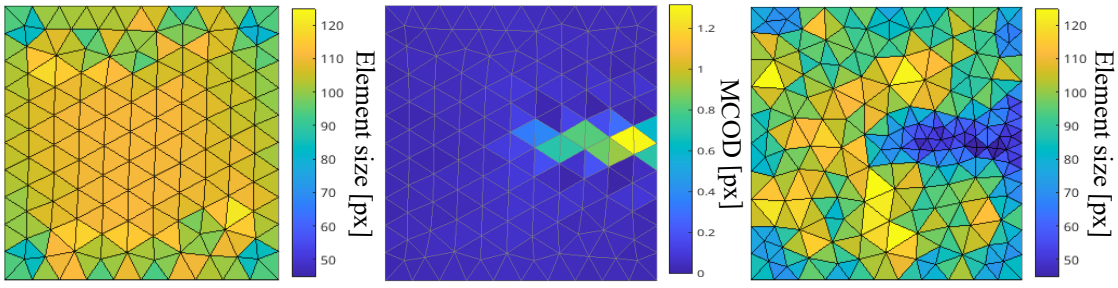

(a) (b) (c)

Figure 2. Mesh refinement at the first iteration. (a) is the element size distribution for the initial mesh; (b) is the MCOD field computed to the same mesh. (c) is the new element size distribution after refinement.

Figure 4 illustrates how the adaptive mesh refinement strategy provides a better resolution of the expected displacement field for the case study. On the left are the results for the initial uniform mesh, and on the right are the same results for the refined one. Figures 4 (a) and 4 (b) illustrate the magnitude of the element size distribution

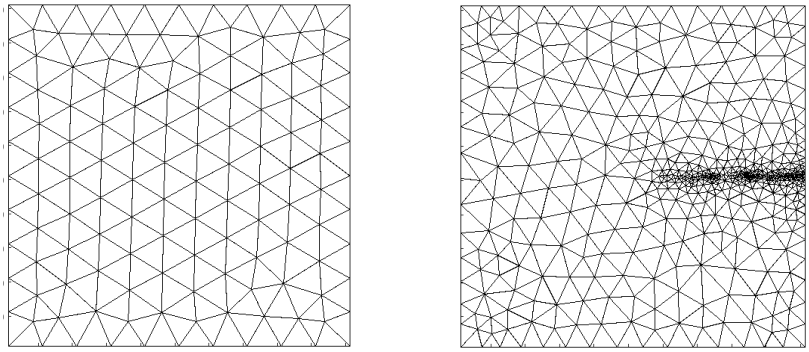

(a) (b)

Figure 3. Initial (a) and final (b) meshes. The last was obtained after four iterations.

between them. Figures 4 (c) and 4 (d) illustrate the displacements field for the vertical component. It is observed that Fig. 4 (d) presents a better definition of the crack region, with displacements compatible with the expected kinematics

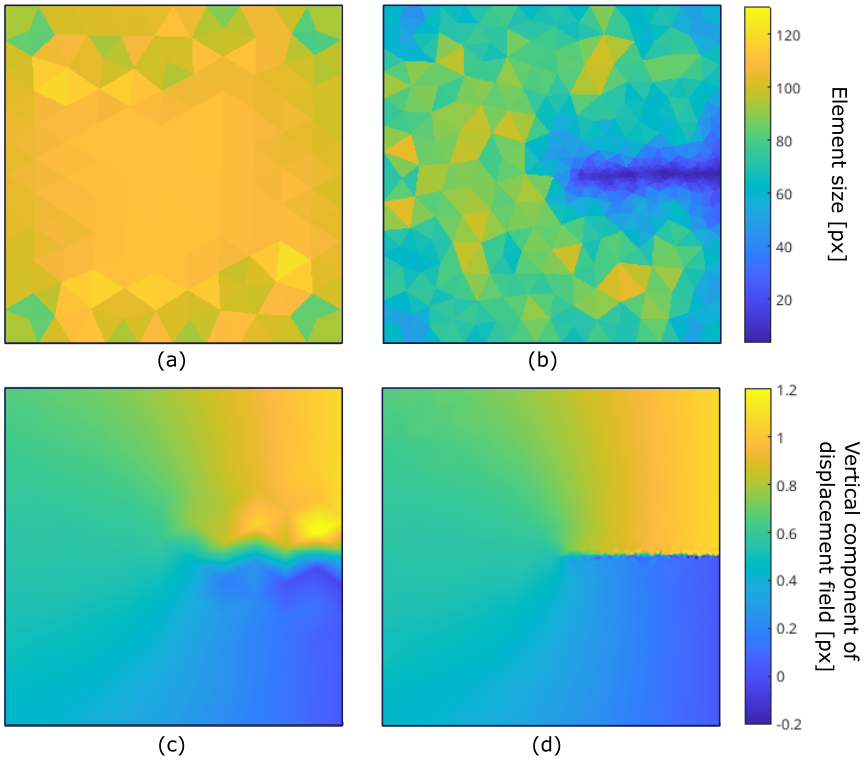

Figure 4. Comparative fields for initial and final meshes. (a) is the element size for the initial mesh; (b) is the element size for the final mesh; (c) is the displacement field for the vertical component of the initial mesh; and (d) is the displacement field for the vertical component of the final mesh.

Fig. 5 compares the initial gray-level residue for the meshes. This value is made dimensionless dividing by the dynamic range, which corresponds to the difference between the maximum and minimum gray level values in the images. The comparison result presents a narrower residual line, better defining the crack location for the refined mesh. Further, Table 1 shows the comparative between the adaptive meshes and uniform meshes, whose mean element sizes were set to be equal to the minimum element size of the adaptive one. For uniform meshes with element sizes lower than 9 px, the DIC analysis diverged, while this size was used on the crack location for the adapted mesh where the analysis fully converged. Probably, the large elements around the smaller ones, for a given adapted mesh, are acting as a regularization scheme, helping the convergence.

Table 1 also shows that adaptive meshes can reduce the residue more than uniform ones, due to the analysis converging to smaller element sizes. The uniform meshes with an average element size inferior to $7.7\mu m$ do not converge. Moreover, Fig. 6 highlights that the number of nodes in adaptive meshes is lower than the one for its analogous uniform meshes (meshes with the smallest element size from adaptive ones). The number of nodes is directly related to the size of the system in the Newton-Raphson algorithm. Thus, it can be associated with the computational cost. The selective refinement provides not only a less costly solution to observe the crack, but also, one that will not increase the residue of uncracked regions, which would occur with a full mesh refinement.

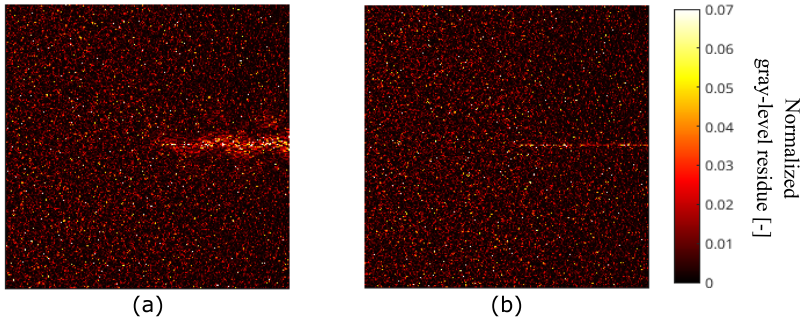

Figure 5. Comparative gray-level residues. (a) initial mesh; (b) refined mesh.

Table 1. Comparison between adaptive mesh (A) and uniform mesh (U), where the minimum element size of the former was set as the mean value of the last.

	Iter 0		Iter 1		Iter 2		Iter 3		Iter 4	
Mesh	A	U	A	U	A	U	A	U	A	U
Residue [%]	1.159	1.140	1.164	1.111	1.102	1.093	1.094	Diverged	1.086	Diverged
ℓ_{max} [px]	120.7	90.2	129.8	60.4	117.3	22.1	114.4	9.2	104.3	4.1
ℓ_{mean} [px]	104.4	79.1	85.7	50.3	68.5	19.9	55.1	7.7	38.0	3.6
ℓ_{min} [px]	79.9	61.5	42.4	21.8	14.5	8.7	9.0	6.6	3.6	2.6

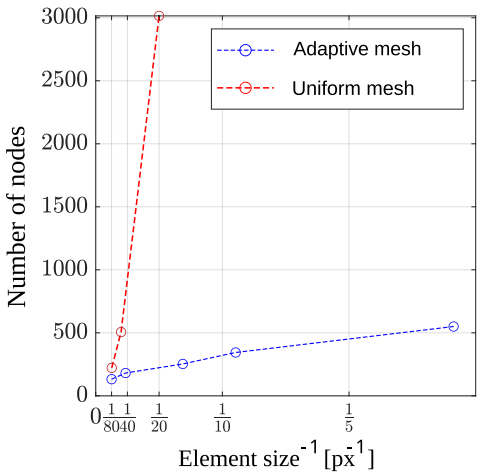

Figure 6. Comparative regarding the number of nodes for uniform and adaptive meshes. For the adapted mesh, the element size is referred to as the minimum; for the uniform mesh, it is the mean value.

6 Conclusions

Implementing mesh refinement in DIC has proven to significantly reduce the global gray-level residue and improve the definition of displacement fields, particularly in regions surrounding cracks. The findings indicate that the normalized gray-level residue decreased from 1.159% with the initial mesh to 1.086% with the final mesh. This substantial reduction highlights the effectiveness of mesh refinement in achieving more accurate displacement measurements.

Moreover, adopting local mesh refinement instead of global refinement has demonstrated a lower computational cost while allowing the use of smaller elements in the regions of interest, reducing the number of nodes by 81.6% in comparison to the uniform mesh with minimum element size that has converged. This refinement strategy is particularly advantageous for improving the identification of displacement fields in areas adjacent to cracks. The improved resolution in these regions is essential for accurately characterizing material behavior, mainly its fracture behavior.

Future investigations should address the potential of varying the refinement parameter (β) to provide further insights into optimizing mesh refinement techniques. Additionally, the effects of other mesh control variables on the mesh refinement algorithm, such as the gray-level residue in each element and maximum principal strain, should be investigated. These research perspectives will enhance fracture mechanic tests assisted by DIC methodologies.

Acknowledgements.

The authors would like to acknowledge the financial support of FAPESP through Processes #2024/05884-9 and #2020/08077-6. Also, to CNPq, for the financial support through Process 140250/2020-4. This study was financed in part by the Coordenação de Aperfeiçoamento de Pessoal de Nível Superior - Brasil (CAPES) - Finance Code 001.

Authorship statement. The authors hereby confirm that they are the sole liable persons responsible for the authorship of this work, and that all material that has been herein included as part of the present paper is either the property (and authorship) of the authors, or has the permission of the owners to be included here.

References

[1] C. Friedrich, R. Gadow, and M. Speicher. Protective multilayer coatings for carbon–carbon composites. *Surface and Coatings Technology*, vol. 151, pp. 405–411, 2002.

[2] W. E. Lee, W. Vieira, S. Zhang, K. G. Ahari, H. Sarpoolaky, and C. Parr. Castable refractory concretes. *International Materials Reviews*, vol. 46, pp. 145–167, 2013.

[3] I. P. Zago, R. Vargas, V. F. Sciuti, R. B. Canto, and R. A. Angélico. Dic to evaluate a model composite system cracking due to cte mismatch. *Theoretical and Applied Fracture Mechanics*, pp. 104330, 2024.

[4] V. F. Sciuti, R. B. Canto, J. Neggers, and F. Hild. On the benefits of correcting brightness and contrast in global digital image correlation: Monitoring cracks during curing and drying of a refractory castable. *Optics and Lasers in Engineering*, vol. 136, 2021a.

[5] L. Wittevrongel, P. Lava, S. V. Lomov, and D. Debruyne. A self adaptive global digital image correlation algorithm. *Experimental Mechanics*, vol. 55, n. 2, pp. 361–378, 2015.

[6] F. Hild and S. Roux. Digital image correlation: from displacement measurement to identification of elastic properties–a review. *Strain*, vol. 42, n. 2, pp. 69–80, 2006.

[7] M. A. Sutton. Computer vision-based, noncontacting deformation measurements in mechanics: a generational transformation. *Applied Mechanics Reviews*, vol. 65, n. 5, pp. 050802, 2013.

[8] G. B. Broggiato and others. Adaptive image correlation technique for full-field strain measurement. In *ICEM12-12th International Conference on Experimental Mechanics*, 2004.

[9] G. Besnard, F. Hild, and S. Roux. "finite-element" displacement fields analysis from digital images: application to portevin–le châtelier bands. *Experimental mechanics*, vol. 46, pp. 789–803, 2006.

[10] V. Sciuti, R. Vargas, R. Canto, and F. Hild. Pyramidal adaptive meshing for digital image correlation dealing with cracks. *Engineering Fracture Mechanics*, vol. 256, pp. 107931, 2021b.

[11] A. Baldi and F. Bertolino. Assessment of h-refinement procedure for global digital image correlation. *Meccanica*, vol. 51, pp. 979–991, 2016.

[12] H. Leclerc, J. Neggers, F. Mathieu, F. Hild, and S. Roux. Correli 3.0. *Iddn. fr*, vol. 1, n. 000, 2015.

[13] C. Geuzaine and J.-F. Remacle. Gmsh: A 3-d finite element mesh generator with built-in pre-and post-processing facilities. *International journal for numerical methods in engineering*, vol. 79, n. 11, pp. 1309–1331, 2009.